Magnetic Resonance Imaging 55 (2019) 128–132

Contents lists available at ScienceDirect

Magnetic Resonance Imaging

journal homepage: www.elsevier.com/locate/mri

Original contribution

Early diagnosis of radio-insensitive human nasopharyngeal carcinoma xenograft models by diffusion kurtosis imaging

Xiang Zheng[a], Yunbin Chen[a,b,*], Youping Xiao[b], Dechun Zheng[b], Weibo Chen[c]

[a] Department of Radiologic Diagnosis, Fujian Medical University Cancer Hospital, Fuzhou, Fujian, China
[b] Department of Radiologic Diagnosis, Fujian Cancer Hospital, Fuzhou, Fujian, China
[c] Philips Healthcare, Shanghai, China

ARTICLE INFO

Keywords:
Nasopharyngeal cancer
Diffusion magnetic resonance imaging
Xenografts
Radiation tolerance

ABSTRACT

Objective: To investigate the feasibility of DKI in early detection of radio-insensitive nasopharyngeal carcinoma (NPC) xenografts in nude mice.

Materials and methods: Seventy-two nude mice were implanted with CNE-1 (low radio-sensitive) and CNE-2 (high radio-sensitive) NPC cell lines, and their respective xenografts were obtained. Then, the NPC-bearing nude mice were exposed to different doses of fraction irradiation, which are divided into non-irradiated group (G0), 10Gy group (G1), 20Gy group (G2), 30Gy group (G3), 3rd (G4) and 5th (G5) days after the entire dose (30y) of irradiation. Subsequently, DKI was performed on each group. Tumor volumes, shrink rates, D and K parameters were measured by two experienced radiologists. Student's *t*-test and receiver operating characteristic (ROC) curve analysis were conducted in this study.

Results: The differences of volume shrinkage rate between CNE-1 and -2 were observed in G2 ($P = 0.032$), with the shrink rates of 5.954% and 27.716%, respectively. The D values were reduced at G1 (D_{G1}, $P = 0.001$) and then increased gradually after irradiation. The K values were increased at G1 (K_{G1}, $P = 0.001$) and then declined sharply in CNE-2 ($P < 0.01$), but not in CNE-1 xenografts ($P > 0.05$). The respective AUC values for D_{G1} and K_{G1} were 0.875 and 0.917, with 66.7% and 83.3% sensitivity and 100% specificity, at the cutoff values of 1.27×10^{-3} mm^2/s for parameter D and 0.88 for parameter K.

Conclusion: DKI can be used for early detection of radio-insensitive NPC xenografts prior to morphological change, where D_{G1} and K_{G1} may be the most valuable indicators.

1. Introduction

Intensity modulated radiation therapy (IMRT) is the main therapeutic strategy for nasopharyngeal carcinoma (NPC), which yields an overall 5-year survival rate of 80% [1]. However, local residual and recurrence still occur in a significant proportion of NPC patients, mainly due to the loss of radio-sensitivity of NPC cells to X-rays. The development of radio-resistance to IMAT has emerged as a major challenge in the treatment of NPC. Thus, an early identification of IMRT radio-resistance is key to develop effective treatment strategies and improve clinical outcomes in NPC patients.

Diffusion weighted (DW) imaging is a non-invasive functional magnetic resonance imaging (MRI) technique that can be used to (i) assess tumor response to anti-cancer therapy; (ii) reflect the changes in tumor metabolism earlier than based on morphological changes; and (iii) predict the treatment outcomes *via* apparent diffusion coefficient (ADC) measurement [2]. However, this imaging model assumes that the diffusion of water molecules obeys Gaussian distribution, where the water diffusion is similar to free diffusion and the diffusion-attenuated DW MR signals follow a mono-exponential pattern. As a result, the actual condition is quite different from assumption, in which the *in vivo* water diffusion is more complicated and displays non-Gaussian behavior. This distribution tends to have a higher peak and heavier tails as compared to the Gaussian distribution of equal mean and variance. Therefore, the model of standard DW imaging may require some improvements, in accordance with the actual displacement distribution of water molecules *in vivo*.

Diffusional kurtosis imaging (DKI) is a DW model first described in 2005, which can measure the non-Gaussian property of water diffusion [3]. The water diffusion *in vivo* is considered to be restricted diffusion

* Corresponding author at: Department of Radiologic Diagnosis, Fujian Cancer Hospital & Fujian Medical University Cancer Hospital, No. 420 Fuma Road, Fuzhou 350014, Fujian, China.
E-mail address: yunbinchen@126.com (Y. Chen).

https://doi.org/10.1016/j.mri.2018.08.001
Received 16 May 2018; Received in revised form 5 August 2018; Accepted 7 August 2018

instead of free diffusion, or in other words, the diffusion of water in tissue is anisotropic. Depending on the nature of its properties, DKI can better reflect the microstructural complexity of tissues [4]. Moreover, DKI can be used to estimate the excess kurtosis of water diffusion *in vivo,* which quantifies the deviation of tissue diffusion from Gaussian pattern and diffusion coefficient is corrected for non-Gaussian bias.

For many years, a great deal of attention has been focused on the DKI imaging of the central nervous system (CNS), including schizophrenia, Alzheimer disease(AD), cerebral infarction, glioma, attention deficit hyperactive disorder, *etc.* [5–9]. More recently, the application of DK imaging has shift away from CNS diseases and move towards cancers, including head and neck tumors. Jansen et al. [10] utilize DKI technique to detect the microstructure of head and neck squamous cell carcinoma, based on non-Gaussian distribution characteristics of water molecules. They found that diffusion kurtosis model and experimental data points fitting degree are higher as compared to the single exponential diffusion model, and the apparent coefficient of kurtosis (Kapp) is about 2 times the apparent diffusion coefficient (Dapp). Moreover, DKI has been shown to be superior to conventional DWI, for the early prediction of refractory NPC [11]. However, there are few reports on the use of DKI for the early prediction of tumor response to IMRT in NPC.

Therefore, our study aimed to investigate the feasibility of DKI in predicting radio-insensitivity of human NPC xenografts in nude mice models. The potential of this imaging technique in the early assessment of tumor response to radiotherapy in NPC xenograft models will serve as a basis for supporting its future clinical application in early detection of radio non-response NPC patients.

2. Materials and methods

2.1. Ethics statement

All experimental procedures were conducted in compliance with institutional guidelines for the care and use of laboratory animals in Fuzhou General Hospital of Nanjing Military Command, Fuzhou, China, and in accordance with the general policies determined by the *National Institutes of Health Guide for Care and Use of Laboratory Animals*.

2.2. Subjects

2.2.1. Construction of human NPC xenograft models

Four weeks old male Balb/C nude mice with immunological deficiency were used in the study. All animals were maintained in a sterile environment, with a relative humidity of 50% and temperature at 25 °C. Both low and high radio-sensitivities NPC cell lines (CNE-2 and CNE-1, respectively) were implanted on the right axilla of nude mice. The xenograft tumors were harvested when they reach 1.5 cm in diameter. A total of 72 nude mice were divided into two groups treated with CNE-1 (n = 36) and CNE-2 (n = 36), respectively. Further, the nude mice in each group were randomly assigned into six groups, for the treatment with fractional irradiation.

2.2.2. Fractional irradiation

All the NPC-bearing nude mice were anesthetized with 7.5 μl/g BW of 5% chloral hydrate by intraperitoneal injection. The surface of nude mice and xenografts were covered by diluted medical alginate, in order to manipulate the radiation exposure dose on tissues. The total dose of fractional irradiation was 30Gy, with 10Gy dose per fraction. Each animal received a single dose of 10 Gy at each time-point, by using a linear accelerator that produced X-ray with a voltage of 6 MV, dose rate of 350 u/min, source and skin distance of 100 cm, and irradiation field size of 3 cm × 3 cm. The treatment conditions for the six groups of nude mice were as follows: (i) G0 group: the non-radiation control group; (ii) G1 group:, the time-point after exposure to 10Gy; (iii) G2 group: the time-point after exposure to 20Gy dose; (iv) G3 group: the time-point after exposure to 30Gy; (v) G4 group: 3 days post-irradiation time-point after exposure to 30Gy; and (vi) G5 group: 5 days post-irradiation time-point after exposure to 30Gy.

2.2.3. MR imaging

The examination of tumor response after fractional irradiation was conducted with both T2WI and DK imaging. All the imaging data were acquired using a clinical 3 T-MRI scanner with parallel imaging (Achieva, Philips) and a special mouse coil. An ice-water phantom was used to validate the values of DK imaging. G0 group received MRI scan without any irradiation. G1, G2, and G3 groups received MRI scan on the next day after irradiated with 10Gy, 20Gy and 30Gy doses, respectively. G4 and G5 groups underwent MRI scans on days 3 and 5, respectively, after receiving the entire dose of 30Gy.

The imaging protocol consists of MRI and DKI sequences:

1. Axial T2-weighted turbo spin-echo (TSE) sequence, with a TR/TE of 1500/180 msec, a slice thickness of 2 mm, an inter-slice gap of 0 mm, a field of view (FOV) of 40 × 40 mm^2, an acquisition matrix of 240 × 240, and a number of excitation (NEX) of 2;
2. Coronal T2-weighted turbo spin-echo (TSE) sequence, with a TR/TE of 1500/180 msec, a slice thickness of 4 mm, an inter-slice gap of 0 mm, a FOV of 80 × 40 mm^2, an acquisition matrix of 240 × 240, and a NEX of 2;
3. Axial DK imaging sequence with five b values (b = 0, 500, 1000, 1500 and 2000 s/mm^2) and three orthogonal motion-probing gradient directions were geometrically averaged to generate isotropic DW (TR/TE of 1000/shortest msec, FOV of 40 × 40 mm^2, acquisition matrix of 64 × 57, slice thickness of 4 mm, and inter-slice gap of 0 mm). The sequence took approximately 16.3 min.

2.2.4. Image analyses

All images were transferred to a dedicated workstation (Extended MR WorkSpace, Philips Medical, Best, Netherlands), and prospectively evaluated by two experienced radiologists with at least 10 years of experience in NPC MRI diagnosis. The DKI sequence data were post-processed by using IDL63 software (IL, Chicago, USA). At first, the regions of interest (ROI) along the lesion on T2WI-STIR images were plotted manually. The area of ROI was kept as large as possible and covered at least two-thirds of the lesion, in order to avoid the necrosis zone. After that, each ROI was copied to D and K diagrams, to generate the corresponding DKI parameter values. The D and K values of G0-G5 which represent mean diffusivity and mean kurtosis were defined as D_{G0}-D_{G5} and K_{G0}-K_{G5}, respectively. The xenograft volumes of G0-G5 (V_{G0}-V_{G5}) were measured in both axial and coronal T2-weighted imaging. The shrink rates of xenografts were calculated according to the equation below: $\text{Shrink rate}_{GX} = (V_{G0} - V_{GX})/V_0 \times 100\%$, where "X" represents the number of group.

2.2.5. Statistical analyses

Statistical analysis was performed by using software SPSS (version 20.0). The inter-rater reliability of each parameter was tested first by spearman correlation test. The average value of each parameter was measured by two radiologists in order to obtain the final value. Means and standard deviations (SD) for DK values of xenografts were calculated from each scan. Continuous variables were compared with Student's *t*-test, to determine the differences of xenografts parameters between the two cell lines. In addition, receiver operating characteristic (ROC) curve analysis was conducted to characterize DKI-derived parameters (D and K) at a given time point. *P* values of < 0.05 were regarded as statistically significant.

Table 1
Spearman correlation coefficient of each parameter measured by the two radiologists in the study.

		Volume	Sig.	D	Sig.	K	Sig.
CNE-1	G0	0.903	0.002	0.935	0.001	0.895	0.001
	G1	0.885	0.011	0.924	0.001	0.874	0.001
	G2	0.867	0.043	0.897	0.008	0.867	0.007
	G3	0.844	0.012	0.874	0.044	0.878	0.015
	G4	0.882	0.045	0.902	0.012	0.922	0.038
	G5	0.866	0.033	0.856	0.005	0.898	0.027
CNE-2	G0	0.926	0.001	0.915	0.001	0.926	0.001
	G1	0.879	0.001	0.909	0.018	0.917	0.017
	G2	0.852	0.005	0.887	0.035	0.871	0.042
	G3	0.839	0.013	0.856	0.016	0.877	0.001
	G4	0.892	0.019	0.912	0.046	0.925	0.019
	G5	0.867	0.025	0.897	0.038	0.898	0.035

3. Results

3.1. The inter-rater reliability of each parameter

Table 1 shows the spearman correlation coefficient of each parameter measured by the two radiologists in the study. The spearman correlation coefficient of tumor volume, D value and K value of the six groups in CNE-1 ranged from 0.844–0.903, 0.856–0.935 and 0.867–0.922 respectively. The spearman correlation coefficient of tumor volume, D value and K value of the six groups in CNE-2 ranged from 0.839–0.926, 0.856–0.915 and 0.871–0.926 respectively. As listed in Table 1, the significance of each correlation coefficient was < 0.05, which suggested that each parameter in the study measured by the two radiologists was reliable.

3.2. Shrink rate of CNE-1 and -2 xenografts during fractional irradiation

Table 2 shows the volumes and shrink rates of both CNE-1 and -2 xenografts receiving multiple fractional irradiation. There was no difference in the baseline volumes between the two groups ($P = 0.242$). Likewise, no significant difference ($P = 0.332$) was observed for the shrink rate between CNE-1 and CNE-2, during the first irradiation (G1). Interestingly, the shrink rates of the two cell-line xenografts (CNE-1 = 5.954% and CNE-1 = 27.716%) were significantly different ($P = 0.032$), during the second irradiation (G2). These findings demonstrated that the tumor sizes of both NPC cell-line xenografts regressed after fractional irradiation, and the differences only appeared after G2.

Table 2
Volumes and shrink rates of CNE-1 and -2 xenografts during fractional irradiation.

	CNE-1	CNE-2	*P* value
Volumes(mm^3)			
G0	313.50 ± 3.98	316.16 ± 2.48	0.242
G1	304.67 ± 5.46	299.79 ± 2.10	0.092
G2	294.83 ± 8.86	247.33 ± 4.71	0.000
G3	255.00 ± 3.46	218.00 ± 3.46	0.000
G4	225.83 ± 2.92	191.33 ± 2.94	0.000
G5	205.83 ± 3.74	122.67 ± 4.54	0.000
Shrink rate[a]			
G1	2.818	5.178	0.332
G2	5.954	21.771	0.032
G3	18.660	31.048	0.004
G4	27.964	39.483	0.000
G5	34.609	61.201	0.000

[a] Shrink rate = $(V_{G0} - V_{GX})/V_{G0} \times 100\%$.

3.3. DKI parameters between CNE-1 and -2 xenografts

Fig. 1 shows the parameter maps of a CNE-2 cell-line xenograft. The changing trend of D and K parameters during fractional irradiation are showed in Fig. 2. The D values of both CNE-1 and -2 xenografts decreased after the first irradiation (G1). Notably, the D values of G1 were significantly lower than of G0 in CNE-2 xenografts ($P = 0.001$), while no significant difference was found for the D values between G0 and G1 in CNE-1 xenografts ($P = 0.785$). As illustrated in Fig. 2A, the D values for both CNE-1 and -2 xenografts increased gradually after the second irradiation (G2). However, no significant difference was observed for the D values between CNE-1 and -2 in G0 ($P = 0.019$). As listed in Table 3, the D values were significantly lower for CNE-2 in G2 ($P < 0.001$) and significantly higher in G4 and G5 ($P < 0.05$ and $P < 0.001$, respectively) as compared to those in CNE-1.

Meanwhile, the K values were increased in both CNE-1 and -2 xenografts, after the first irradiation (G1). As similar to D values, a statistically significant difference was observed for the K values between G0 and G1 in CNE-1 xenografts ($P = 0.001$), but not in CNE-2 xenografts ($P = 0.143$). As shown in Fig. 2B, the K values for both xenografts declined sharply after the second irradiation (G2). Furthermore, the K values of G0 and G1 were significantly higher in CNE-2 than in CNE-1 ($P < 0.01$), but were significantly lower in other groups ($P < 0.001$) (Table 2).

3.4. Diagnostic performance for predicting radio-insensitive xenografts

D_{G1} and K_{G1} parameters are the major characteristics that distinguish CNE-1 from CNE-2, due to the temporarily reverse change in G2 of CNE-2 xenografts. In addition, G1 is the critical time-point for tumor size changes before entering G2. Therefore, D_{G1} and K_{G1} are the most appropriate parameters for early prediction of radio-insensitive xenografts. Fig. 3 shows the ROC curves of the two parameters in predicting radio-insensitive xenografts. The area under the curve (AUC) value of D_{G1} was 0.875, with 66.7% sensitivity and 100% specificity, when $D_{G1} > 1.27 \times 10^{-3}\,mm^2/s$. Meanwhile, the AUC value of K_{G1} was 0.917, with 83.3% sensitivity and 100% specificity, when $K < 0.88$.

4. Discussion

Tumor cells proliferate more rapidly than normal cells, and thus attributed to the higher cell density. Indeed, the distribution of water molecules in tumor tissues is obviously lower than in normal tissues. DWI is a functional MRI technique, which has been applied in clinical settings to predict disease. DWI can detect the diffusion of water molecules *in vivo* by obeying Gaussian distribution, and the low ADC value is mainly a consequence of increased cellular density and decreased interstitial space [12,13]. Actual conditions, however, are generally different from those defined by Gaussian distribution, due to the microstructure of tissues such as cells, blood vessels, *etc.* Hence, the diffusion parameters of DWI possess a certain degree of bias. On the contrary, DKI parameters assume that water molecules diffuse according to non-Gaussian distribution, and thus reflect the actual diffusion of water molecules *in vivo* by considering the factors of microcirculation, membrane water channels, cellular density, extracellular space, *etc.* Therefore, in this study, we used DKI to predict the radiation sensitivity of human NPC xenografts in nude mice.

Tumors with radio-resistance are inherently less sensitive to radiation, and tend to shrink more slowly during radiotherapy. In this study, we observed that the volume of NPC xenografts regressed after fractional irradiation. At first, there was no difference on the tumor volume reduction rate between the two cell lines. Upon the second irradiation, we found that the shrinkage rate of CNE-2 was significantly higher than that of CEN-1. These findings suggested that the radio-sensitivity of the two NPC xenografts is not possible to be differentiated before the second irradiation. After the initial exposure to radiation, even at a

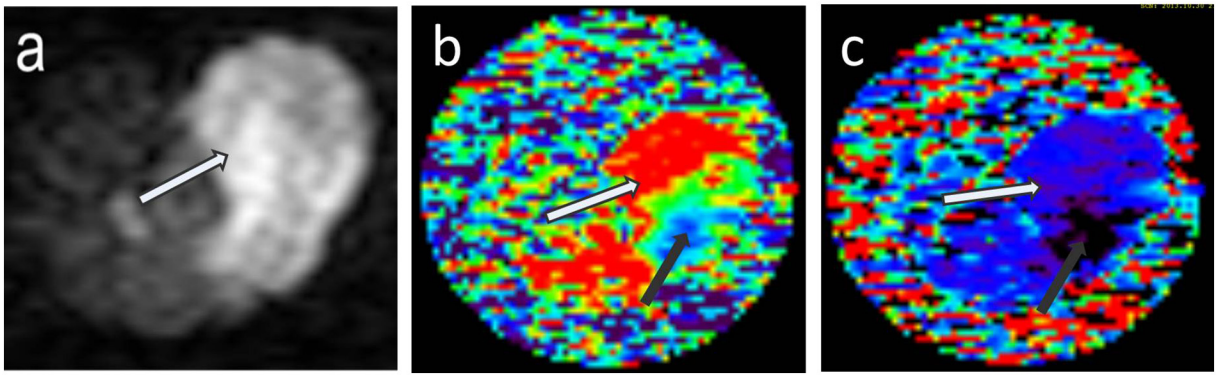

Fig. 1. Representative images of a CNE-2 cell-line xenograft. Picture a-c represents DWI (b = 1000), D and K map, respectively. The xenograft in DWI picture showed as high signal (white arrow, picture a). Most area of xenograft show as red in D map (white arrow, picture b) and dark blue in K map (white arrow, picture c). The blue area in D map (black arrow, picture b) and black area in K map (black arrow, picture c) represent the necrosis area in xenograft which can't be showed clearly in DWI map. (For interpretation of the references to colour in this figure legend, the reader is referred to the web version of this article.)

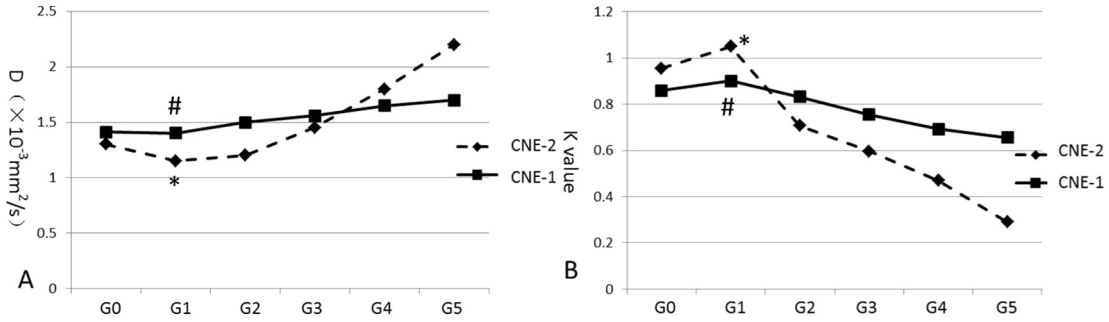

Fig. 2. The changes in D and K values during fractional irradiation
*: $P < 0.05$ v.s. G0 #: $P > 0.05$ v.s. G0.

Table 3
The values and the comparison of D and K between CNE-1 and CNE-2 during fractional irradiation.

		CNE-1	CNE-2	*P*
D($\times 10^{-3}$ mm^2/s)	G0	1.42 ± 0.21	1.32 ± 0.07	0.302
	G1	1.40 ± 0.20	1.15 ± 0.09	0.019
	G2	1.51 ± 0.11	1.21 ± 0.06	0.000
	G3	1.56 ± 0.13	1.45 ± 0.05	0.099
	G4	1.66 ± 0.08	1.80 ± 0.09	0.017
	G5	1.70 ± 0.02	2.24 ± 0.10	0.000
K	G0	0.86 ± 0.06	0.95 ± 0.04	0.009
	G1	0.91 ± 0.04	1.06 ± 0.08	0.002
	G2	0.83 ± 0.05	0.70 ± 0.04	0.001
	G3	0.76 ± 0.06	0.59 ± 0.04	0.000
	G4	0.69 ± 0.08	0.47 ± 0.03	0.000
	G5	0.65 ± 0.05	0.29 ± 0.02	0.000

reduced dose, the cell membrane can be damaged and lead to the dysfunction of active transmembrane transportation of water molecules [14]. Anyhow, the water molecules from extracellular space can still pass through the cell membrane *via* passive transportation, thereby resulting in an increase of intracellular water content and cell density. As a consequence, extracellular space becomes more compact and further restricting the diffusion of the extracellular water molecules.

An increased dose of radiation can lead to the initiation of apoptosis in xenograft cells [15]. The decreased number of tumor cells would result in a lower cell density and followed by an enlargement of extracellular space. Larger extracellular space after cell apoptosis may lead to isotropic microenvironment. Apparently, an induction of D value and reduction of K value were observed during the fractional irradiation of CNE-1 and -2 xenografts. In xenografts of CNE-2 cell-line, D and K values transient changed reversely after the first irradiation, but similar changes were not observed in CNE-1 xenografts. The radiosensitive of CNE-2 is higher than CNE-2, and therefore the temporarily reverse changes in D and K values during the initial stage of fraction irradiation (G1) are clearly observed prior to morphological changes. Similarly, the use of diffusional MR on head and neck squamous cell carcinoma, hepatic metastases and metastatic ovarian cancer have shown that the changes of MRI diffusional imaging biomarkers are often earlier than that of tumor size [16–18]. Hence, the temporarily reverse changes in D and K values may differentiate the micro-environment of G1 between radio-sensitive and -insensitive NPC xenografts. The respective AUC values of D_{G1} and K_{G1} were 0.875 and 0.917, with 66.7% and 83.3% sensitivity and both 100% specificity, at the cutoff values 1.27×10^{-3} mm^2/s for parameter D and 0.88 for parameter K. These results indicated that the NPC cells may be radioresistance, when $D_{G1} > 1.27 \times 10^{-3}$ mm^2/s or $K_{G1} < 0.88$. Therefore, both D_{G1} and K_{G1} are the most valuable imaging markers for the early detection of radio-sensitivity in NPC xenografts.

Furthermore, Jansen et al. [10] found that Kapp is twice as high as Dapp in head and neck squamous cell carcinoma and the lymph node. Obviously, the fitting degree of DKI parameters constructed from both double exponential model and experimental data is higher than that of DWI parameters constructed from single exponential model. Chen et al. [12] also proposed that the D value of DKI and the ADC value of DWI can both predict the efficacy of NPC chemotherapy, in which the D and K parameters are superior to the ADC parameter. In fact, ADC parameter has been proposed as a valuable indicator for the early assessment of tumor response to radiation therapy in NPC [19,20]. Notably, the low pre-treatment ADC values in tumor tissues may contribute to better treatment outcomes [21,22]. Nevertheless, Chen et al. [11] found that K values are not significantly different between the response and non-response groups during neoadjuvant chemotherapy of NPC. The reasons for this are twofold; (i) the effects of radiotherapy and

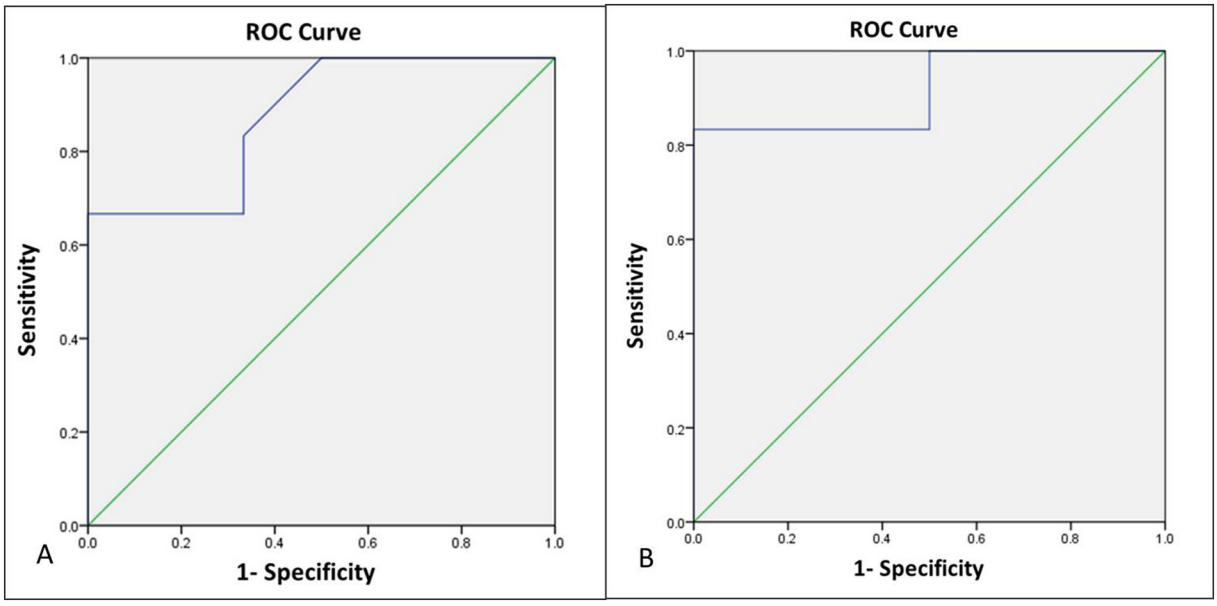

Fig. 3. ROC curves of DG1 and KG1 in picture A and B. The areas under the curve are 0.875 and 0.917, with sensitivity of 0.667 and 0.833 as well as specificity of 1.000 and 1.000, respectively.

chemotherapy on the ultrastructure of tumor tissues might be different; and (ii) the complexity of tumor tissue is influenced by cell density, uniformity of cell distribution, structure of tissue, *etc.*

5. Conclusions

The results of this study indicate that DKI has the potential to predict the radio-sensitivity in human NPC xenografts prior to morphological alterations. In addition, D_{G1} and K_{G1} may be the most useful parameters for early prediction of tumor response to radiotherapy. However, the impacts of D and K values on the long-term survival and recurrence risk of NPC have not been elucidated. Therefore, the findings from this *in vivo* study should be further confirmed in adequately designed prospective clinical trials.

References

[1] Lee AW, Ng WT, Chan LL, et al. Evolution of treatment for nasopharyngeal cancer–success and setback in theintensity-modulated radiotherapy era. Radiother Oncol 2014;110(3). [377-4].
[2] Chen YB, Liao J, Xie R, et al. Discrimination of metastatic from hyperplastic pelvic lymph nodes in patients with cervical cancer by diffusion-weighted magnetic resonance imaging. Abdom Imaging 2011;36(1):102–9.
[3] Jensen JH, Helpern JA, Ramani A, et al. Diffusional kurtosis imaging: the quantification of non-Gaussian water diffusion by means of magnetic resonance imaging. Magn Reson Med 2005;53(6):1432–40.
[4] Lu H, Jensen JH, Ramani A, et al. Three-dimensional characterization of nonGaussian water diffusion in humans using diffusion kurtosis imaging. NMR Biomed 2006;19(2):236–47.
[5] Ramani A, Jensen JH, Szulc KU, et al. Assessment of abnormalities in the cerebral microstructure of schizophrenia patients: a diffusional kurtosis imaging study. Proc Intl Soc Mag Reson Med 2007;15:648.
[6] Lu H, Jensen JH, Hu C, et al. Alterations in cerebral microstructural integrity in normal aging and in Alzheimer's Disease: a multi-contrast diffusion MRI Study. Proc Intl Soc Mag Reson Med 2006;14:723.
[7] Falangola MF, Jensen JH, Babb JS, et al. Age relatednon Gaussian diffusion patterns in the prefrontable brain. J Magn Reson Imaging 2013;28(6):1345–50.
[8] Helpern JA, Adisetiyo V, Falangola MF, et al. Preliminary evidence of altered gray and white matter microstructural development in the frontal lobe of adolescents with attention-deficit hyperactivity disorder: a diffusional kurtosis imaging study. J Magn Reson Imaging 2011;33:17–23.
[9] Raab P, Hattingen E, Franz K, et al. Cerebral gliomas: diffusional kurtosis imaging analysis of microstructural differences. Radiology 2010;254:876–81.
[10] Jansen JF, Stambuk HE, Koutcher JA, et al. Non Gaussian analysis of diffusion weighted MR imaging in head and neck squamous cell carcinoma: a feasibility study. AJNR Am J Neuroradiol 2010;31(4):741–8.
[11] Chen Y, Ren W, Zheng D, et al. Diffusion kurtosis imaging predicts neoadjuvant chemotherapy responses within 4 days in advanced nasopharyngeal carcinoma patients. J Magn Reson Imaging 2015 Nov;42(5):1354–61.
[12] Barajas Jr. RF, Rubenstein JL, Chang JS, et al. Diffusion-weighted MR imaging derived apparent diffusion coefficient is predictive of clinical outcome in primary central nervous system lymphoma. AJNR Am J Neuroradiol 2010;31:60–6.
[13] Lambrecht M, Dirix P, Vandecaveye V, et al. Role and value of diffusion-weighted MRI in the radiotherapeutic management of head and neck cancer. Expert Rev Anticancer Ther 2010;10:1451–9.
[14] Freeman A, Hetzel U, Cripps P, et al. Expression of the plasma membrane markers aquaporin 1 (AQP1), glucose transporter 1 (GLUT1) and Na^+-K^+-ATPase in canine mammary glands and mammary tumours. Vet J Jul 2010;185(1):90–3.
[15] Ou G, Itasaka S, Zeng L, et al. Usefulness of HIF-1 imaging for determining optimal timing of combining bevacizumab and radiotherapy. Int J Radiat Oncol Biol Phys 2009;75(2):463–7.
[16] Thoeny HC. Diffusion-weighted MRI in head and neck radiology: applications in oncology. Cancer Imaging 2011;10:209–14.
[17] Bains LJ, Zweifel M, Thoeny HC. Therapy response with diffusion MRI: an update. Cancer Imaging 2012;12:395–402.
[18] Vandecaveye V, Dirix P, De Keyzer F, et al. Predictive value of diffusion weighted magnetic resonance imaging during chemoradiotherapy for head and neck squamous cell carcinoma. Eur Radiol 2010;20:1703–14.
[19] Pan J, Zang L, Zhang Y, et al. Early changes in apparent diffusion coefficients predict radiosensitivity of human nasopharyngeal carcinoma xenografts. Laryngoscope 2012;122(4):839–43.
[20] Hong J, Yao Y, Zhang Y, et al. Value of magnetic resonance diffusion-weighted imaging for the prediction of radiosensitivity in nasopharyngeal carcinoma. Otolaryngol Head Neck Surg Nov 2013;149(5):707–13.
[21] Koh DM, Scurr E, Collins D, et al. Predicting response of colorectal hepatic metastasis: value of pretreatment apparent diffusion coefficients. AJR Am J Roentgenol Apr 2007;188(4):1001–8.
[22] Song I, Kim CK, Park BK, et al. Assessment of response to radiotherapy for prostate cancer: value of diffusion-weighted MRI at 3 T. AJR Am J Roentgenol Jun 2010;194(6):W477–82.